Nonlinear coupling between cerebral blood flow, oxygen consumption, and ATP production in human visual cortex

Ai-Ling Lin[a,b,1], Peter T. Fox[a,b,c,d,e], Jean Hardies[a], Timothy Q. Duong[a,c,d,e,f], and Jia-Hong Gao[g,1]

[a]Research Imaging Institute and Departments of [b]Psychiatry, [c]Radiology, and [d]Physiology, University of Texas Health Science Center at San Antonio, San Antonio, TX 78229; [e]South Texas Veterans Health Care System, Department of Veterans Affairs, San Antonio, TX 78229; [f]Department of Ophthalmology, University of Texas Health Science Center at San Antonio, San Antonio, TX 78229; and [g]Departments of Radiology, Psychiatry, and Behavioral Neuroscience, and Brain Research Imaging Center, The University of Chicago, Chicago, IL 60637

Edited by Marcus E. Raichle, Washington University, St. Louis, MO, and approved March 30, 2010 (received for review September 4, 2009)

The purpose of this study was to investigate activation-induced hypermetabolism and hyperemia by using a multifrequency (4, 8, and 16 Hz) reversing-checkerboard visual stimulation paradigm. Specifically, we sought to (*i*) quantify the relative contributions of the oxidative and nonoxidative metabolic pathways in meeting the increased energy demands [i.e., ATP production (J_{ATP})] of task-induced neuronal activation and (*ii*) determine whether task-induced cerebral blood flow (CBF) augmentation was driven by oxidative or nonoxidative metabolic pathways. Focal increases in CBF, cerebral metabolic rate of oxygen ($CMRO_2$; i.e., index of aerobic metabolism), and lactate production (J_{Lac}; i.e., index of anaerobic metabolism) were measured by using physiologically quantitative MRI and spectroscopy methods. Task-induced increases in J_{ATP} were small (12.2–16.7%) at all stimulation frequencies and were generated by aerobic metabolism (approximately 98%), with $\%\Delta J_{ATP}$ being linearly correlated with the percentage change in $CMRO_2$ ($r = 1.00$, $P < 0.001$). In contrast, task-induced increases in CBF were large (51.7–65.1%) and negatively correlated with the percentage change in $CMRO_2$ ($r = -0.64$, $P = 0.024$), but positively correlated with $\%\Delta J_{Lac}$ ($r = 0.91$, $P < 0.001$). These results indicate that (*i*) the energy demand of task-induced brain activation is small (approximately 15%) relative to the hyperemic response (approximately 60%), (*ii*) this energy demand is met through oxidative metabolism, and (*iii*) the CBF response is mediated by factors other than oxygen demand.

cerebral metabolic rate of oxygen | lactate production

The physiological mechanisms underlying task-induced, focal increases in brain blood flow have been a matter of speculation, experimentation, and debate for more than a century. Roy and Sherrington opened the dialogue with the observation that "the brain possesses an intrinsic mechanism by which its vascular supply can be varied locally in correspondence with local variations of functional activity" (1) and attributed these to vasodilatory properties of "the chemical products of cerebral metabolism" (1), with the presumption that metabolism was focally increased by neuronal activity. The Roy–Sherrington principle has been interpreted to mean that blood flow changes must be a function of a tight coupling between cellular energy requirements and the supplies of glucose and oxygen. Studies using preimaging radiotracer techniques demonstrated that brain blood flow can be markedly elevated by increased partial pressure of CO_2 and by decreased partial pressure of O_2, a form of cerebrovascular autoregulation (2). These observations provided strong support for the Roy–Sherrington principle, as CO_2 is the primary "chemical product" of glucose oxidation, and extended the hypothesis to include substrate ($[O_2]$) availability as a potent vascular regulator.

The first imaging-based measurements of cerebral metabolic rate of O_2 ($CMRO_2$) during task performance were reported in the early 1980s, using ^{15}O positron emission tomography (PET) (3, 4). In two different brain systems (visual and somatosensory), Fox et al. observed that task-induced increases in $CMRO_2$ were much lower than those in cerebral blood flow (CBF) and cerebral metabolic rate of glucose (CMR_{Glc}) (5, 6). The $CMRO_2$ shortfall during focal neuronal activation, in fact, caused a local oxygen surplus, with the oxygen extraction fraction (OEF) decreasing from a resting value of approximately 40% to a task-state value of approximately 20%. That is, 80% of the oxygen delivered during task performance was not metabolized. These findings clearly contradicted the Roy–Sherrington principle. Fox and colleagues suggested that (*i*) the energy demand associated with neuronal activation (as opposed to resting-state demand) is small (approximately 8% maximum possible increase in ATP consumption), (*ii*) the activation-induced increases in ATP consumption are from both oxidative and nonoxidative glycolysis, and (*iii*) CBF response must be regulated by factors other than oxidative metabolism and total energy demand. In later studies, CBF increase was observed to be modulated by byproducts of nonoxidative metabolism, such as lactate production (J_{Lac}) (7). The observation that the stimulus-evoked increase in glucose consumption observed with PET is at least partially nonoxidative (i.e., lactate-producing) has been confirmed with ^1H NMR spectroscopic (MRS) measurements of tissue lactate concentration ([Lac]) (8, 9). Such uncoupling of CBF and $CMRO_2$ is the basis for the blood oxygenation level–dependent (BOLD) functional MRI (fMRI) contrast (10, 11).

During the past decade, fMRI techniques have been developed that enable physiological investigations of activation-induced hyperemia and hypermetabolism. Stimulus-evoked $CMRO_2$ change ($\%\Delta CMRO_2$) between rest and activated states has been reported based on the biophysical BOLD model (12). In this BOLD model, $\%\Delta CMRO_2$ is computed based on the task-induced changes of physiological parameters—oxygenation (i.e., BOLD), CBF, and cerebral blood volume (CBV)—and basal BOLD relaxation rate (M) via hypercapnic calibration (Eq. **1**). All these parameters can be measured by MRI in a single setting. In the majority of fMRI studies, stimulus-evoked $CMRO_2$ changes and the flow–metabolism coupling relationship observed contradicted earlier PET observations (5, 6, 13–15). Specifically, with a similar neuronal stimulation, fMRI-measured $\%\Delta CMRO_2$ was much higher than that of PET (20–30% vs. 5–10%). The relationship between task-induced $\%\Delta CMRO_2$ and CBF change ($\%\Delta CBF$) determined by fMRI appeared linear, i.e., with a constant ratio ($\%\Delta CBF$:$\%\Delta CMRO_2$, approximately 2:1) regardless of the stimulus intensity (14,

Author contributions: A.-L.L. and J.-H.G. designed research; A.-L.L. performed research; J.H. contributed new reagents/analytic tools; A.-L.L. analyzed data; and A.-L.L., P.T.F., T.Q.D., and J.-H.G. wrote the paper.

The authors declare no conflict of interest.

This article is a PNAS Direct Submission.

Freely available online through the PNAS open access option.

[1]To whom correspondence may be addressed. E-mail: lina3@uthscsa.edu or jgao@uchicago.edu.

www.pnas.org/cgi/doi/10.1073/pnas.0909711107

15). However, a linear (i.e., with constant slope) flow–metabolism relationship was observed by PET only in the resting state (with a slope of approximately 0.97; ref. 6). During activation, a nonlinear coupling between %ΔCBF and %$\Delta CMRO_2$ was observed, with a coupling ratio that varied from 2 to 10 (5, 13). The discrepancy between PET and fMRI observations on flow–metabolism coupling during task was an obstacle to the further understanding of metabolic physiology for more than a decade. This discrepancy, however, recently has been resolved (16, 17). It is now clear that the discrepancy was due to incorrect simplifying assumptions of the fMRI model, as follows.

In most fMRI studies of CBF:$CMRO_2$ coupling, CBV was not measured and was instead estimated from CBF under the assumption that CBV and CBF have a constant power-law relationship (18). However, it has been shown the CBV–CBF relationship is not fixed during neuronal activation and rather changes with stimulus frequency and duration (19, 20). This erroneous assumption allowed $CMRO_2$ determinations to be incorrectly determined by CBF, necessarily showing a linear CBF:$CMRO_2$ relationship. An additional error made by semi-quantitative fMRI studies of CBF:$CMRO_2$ coupling was overestimating the M value, which causes overestimation of %Δ$CMRO_2$. By explicitly measuring each of the physiological parameters (CBV, CBF, and BOLD) and carefully determining the M value, we have found that the fMRI BOLD model yields %Δ$CMRO_2$ values and a nonlinear flow–metabolism relationship (coupling ratio ranging from 2 to 8), in close agreement with the PET literature (16, 17).

With the revised model, we revisited the widely debated issue of flow–metabolism coupling during task-induced brain activation. In doing so, we employed explicit CBV measurements and rigorous M-value determination, and also concurrently measured task-induced changes in lactate by using ^{1}H MRS to differentiate the aerobic and anaerobic metabolic pathways. Specifically, we sought to (*i*) determine whether task-induced CBF augmentation was regulated by oxidative or nonoxidative metabolic pathways and (*ii*) quantify the relative contributions of oxidative and nonoxidative metabolic pathways in meeting the increased energy demands [ATP production (J_{ATP})] of task-induced neuronal activation. The J_{ATP} was determined by a stoichiometric relationship between changes of $CMRO_2$ and J_{Lac}. A secondary goal of the study was to link our MRI results to current physiological hypotheses that are alternatives to the Roy–Sherrington principle. In this study, we induced focal activation using reversing checkerboard stimulation at three different frequencies: 4, 8, and 16 Hz. This paradigm was selected because it has been shown to reliably produce variable degrees of "uncoupling" between CBF and $CMRO_2$ (13, 16), with 4 Hz being more "coupled" than 8 or 16 Hz. All measurements were made in the same subjects and in the same sessions to minimize errors.

Results

MRI and MRS Results. The group-averaged (n = 12) %ΔBOLD, %ΔCBF, and CBV change (%ΔCBV) are shown in Table 1. The magnitudes of the three quantities were increased in response to stimulation peaking at 8 Hz, in agreement with previous studies (11, 13, 21). The basal BOLD relaxation rate (i.e., M value) determined from hypercapnic challenge was 0.093 ± 0.003. The magnitude of $CMRO_2$ increase in response to the stimulation reached a maximum at 4 Hz (Table 1). Locations and percentage changes in CBF and $CMRO_2$ at the three stimulus frequencies in primary visual cortex are shown in Fig. 1. In vivo ^{1}H NMR spectra acquired from the visual cortex during rest and three stimulation periods are shown in Fig. 2. The lactate peaks were visible at 1.33 ppm. Maximal [Lac] change (%Δ[Lac]) was also observed at 8 Hz (Table 1). The %ΔJ_{Lac} at each condition was determined by %Δ[Lac] over a period of 4 min (Table 1). Basal J_{Lac} [$J_{Lac(r)}$] determined by Eq. **3** was 0.27 μmol/g/min. The magnitudes of lactate production at the three levels of stimulation [$J_{Lac(a)}$] were then calculated as $J_{Lac(r)} \times (1 + \%\Delta J_{Lac})$. For all variables measured, response magnitudes differed significantly across stimulation conditions (Table 1), with less uncoupling at 4 Hz than at 8 or 16 Hz. The most marked dissociation was in OEF (F = 73.6, $P = 6.9 \times 10^{-13}$), which confirmed the remarkable uncoupling between $CMRO_2$ and CBF at higher stimulation rates (13, 16).

J_{ATP}: Aerobic Versus Anaerobic Contributions. A $J_{ATP(r)}$ of 11.1 μmol/g/min was determined from basal $CMRO_2$ [$CMRO_{2(r)}$] and CMR_{Glc} [$CMR_{Glc(r)}$] (Eq. **2**) (5, 22). Steady-state J_{ATP} at each activated condition [$J_{ATP(a)}$] was determined from the stoichiometric relationships between %ΔJ_{Lac} and %Δ$CMRO_2$ (Eq. **5**) (22). The results showed that the $J_{ATP(a)}$, both absolute quantification (in μmol/g/min) and relative changes (as a percentage), were not significantly different among the three stimulus frequencies ($P > 0.5$; Table 2 and Fig. 3*A*). The ΔJ_{ATP} range of 1.4 to 1.9 μmol/g/min confirmed those reported previously in the PET literature (see summary in ref. 22). The J_{ATP} percent contributions from aerobic and anaerobic metabolism were then computed. The %ΔJ_{Lac} contribution was considered anaerobic, whereas %Δ$CMRO_2$ was aerobic. As expected, $J_{ATP(a)}$ was predominantly caused by oxidative metabolism (approximately 98%) at 4 Hz, which represents the lowest %ΔJ_{Lac} and highest %Δ$CMRO_2$ of the three stimuli. Assuming 7% to 14% of $J_{ATP(a)}$ was contributed by astrocytes (23, 24), it was deduced that neurons contribute 84% to 91%. Interestingly, a similar result of approximately 98% oxidative contribution in total to $J_{ATP(a)}$ was also seen at 8 and 16 Hz, even though %Δ[Lac] increased while %Δ$CMRO_2$ decreased (Table 2 and Fig. 3*B*). The %ΔJ_{ATP} was thus shown to tightly correlate with %Δ$CMRO_2$ (r = 1.00, $P < 0.001$; Fig. 4*A*).

Comparison of %ΔCBF Versus %ΔJ_{Lac} and %Δ$CMRO_2$. As demonstrated in Table 1, both %ΔCBF and %Δ[Lac] (an approximation of %ΔJ_{Lac}) reached their maximum at 8 Hz. As a result, %ΔCBF was highly correlated with %ΔJ_{Lac} (r = 0.91, $P < 0.001$; Fig. 4*B*). In contrast, %Δ$CMRO_2$ reached a maximum at 4 Hz. As a result, nonlinear coupling and a negative correlation was found between %ΔCBF and %Δ$CMRO_2$ (r = −0.64, Fig. 4*C*). The observed relationship between %ΔCBF and %Δ$CMRO_2$ in this work is consistent with most recent fMRI and PET findings

Table 1. Variables obtained with fMRI and ^{1}H MRS for each of the visual stimulation rates

Rate	ΔBOLD, %	ΔCBV, %	ΔCBF, %	Δ$CMRO_2$, %	ΔOEF, %	Δ[Lac], %	ΔJ_{Lac}, %
4 Hz	1.8 ± 0.4	19.0 ± 4.6	51.7 ± 7.8	17.0 ± 3.3	−22.7 ± 1.4	31.3 ± 4.4	7.8 ± 1.1
8 Hz	2.5 ± 0.2	28.5 ± 3.8	65.1 ± 5.9	13.4 ± 4.0	−31.2 ± 1.9	50.0 ± 5.7	12.5 ± 1.5
16 Hz	2.3 ± 0.3	24.8 ± 5.1	57.2 ± 6.2	12.2 ± 4.1	−28.9 ± 2.3	46.1 ± 4.7	11.5 ± 1.2
F	24.2***	24.3***	13.5**	5.8*	73.6****	25.8***	25.8***
Post hoc	4 << 8 = 16	4 << 8 = 16	4 << 8 = 16	4 < 8 = 16	4 << 8 = 16	4 << 8 = 16	4 << 8 = 16

Values are means ± SD. *F* values were computed by one-way, repeated measures ANOVA, ****$P < 10^{-12}$, ***$P < 10^{-6}$, **$P < 0.001$, *$P < 0.01$. Post-hoc testing was performed per condition by Newman-Keuls test, where << indicates $P < 0.001$, < indicates $P < 0.01$, and = indicates $P > 0.5$.

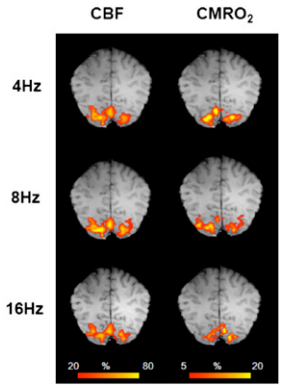

Fig. 1. The location and magnitude of %ΔCBF and %ΔCMRO$_2$ in primary visual cortex during 4-, 8-, and 16-Hz visual stimulation.

(16, 17, 25, 26). In addition, %ΔCBF correlated to a greater degree with %ΔJ$_{Lac}$ ($P < 0.001$) than %ΔCMRO$_2$ ($P = 0.024$).

Discussion

The major findings were that (*i*) task-induced increases in oxygen metabolism and energy demand were small (12–17%), (*ii*) oxidative (indexed by CMRO$_2$) and nonoxidative (indexed by lactate production) metabolism coexisted during visual stimulation, and (*iii*) CBF increases were much larger (52–65%) than the increases in energy demand and were highly correlated ($r = 0.91$) with lactate production, but not with CMRO$_2$. The first observation was consistent with prior PET findings (13, 25). The second observation (i.e., increase in nonoxidative metabolism) echoed previous MRS results (8, 9). The third observation was in line with PET results (5, 13) but disagreed with fMRI studies that made the assumptions discussed earlier (14, 15) and with the Roy–Sherrington principle. Further, the conclusion of J$_{ATP}$ being met through oxidative metabolism was in good agreement with previous fMRI literature (14, 15), but not with PET literature (5, 6)

Collectively, the functional imaging literature (PET, fMRI, and MRS) has forced the development of alternatives to the Roy–Sherrington hypothesis. Of these, the astrocyte–neuron lactate shuttle (ANLS) hypothesis is the most conceptually evolved and widely accepted (27). The ANLS hypothesis posits a cooperation between neurons and glia in meeting the activation-induced needs for energy production (i.e., ATP production) and for neurotransmitter production, as follows (ref. 27 and figure 4 in ref. 23). Upon neuronal firing, glucose is taken up and metabolized in neurons and astrocytes. The majority of the glucose is taken up by the astrocytes; the remainder by neurons (23). Glucose consumption in neurons is small but entirely oxidative (23, 28). Astrocytic glucose consumption, conversely, is large but much less efficient by virtue of being predominantly glycolytic (29). Astrocytic glycolysis supports Na^+/K^+ ion pumping and glutamate-glutamine (Glu-Gln) conversion. Glial lactate (produced by glycolysis) is eventually transported to neurons as fuel, but with some loss into the circulation, which increases hyperemia (7). The ANLS hypothesis implies that (*i*) increases in CMR$_{Glc}$ are for purposes other than oxygen demand, e.g., for astrocyte-mediated neurotransmitter recycling; (*ii*) task-induced oxygen demand is small; and (*iii*) CBF increases are regulated by factors other than oxidative metabolism.

Our three findings were in good agreement with the ANLS hypothesis. The first finding (i.e., small CMRO$_2$ increase) is in line with the ANLS implication that the energy demands of acute, transient increases in neuronal activity are small (approximately 15% increase in CMRO$_2$ at most) (30). One speculation is that mitochondrial cytochrome oxidase activity is regulated by chronic energy requirements, averaged over long periods of time (31, 32). Consequently, surge increases in neuronal activity cannot be accompanied by large increases in oxygen consumption. Specifically, the increases in ATP production during transient neuronal activations cannot be large (33), as in the present study (12–17%). As neuronal activation continues, based on the ANLS hypothesis, oxidative metabolism is expected to increase as a result of the uptake of glially produced lactate into the tricarboxylic acid cycle by the neurons as a fuel substrate. In support of this formulation, prolonged visual stimulation (>20 min) has been reported to induce gradually rising levels of CMRO$_2$ and gradually decreasing CMR$_{Glc}$ and J$_{Lac}$ (8, 16, 26, 34, 35).

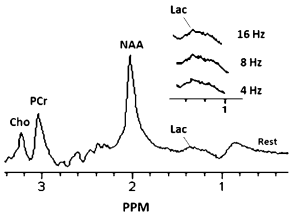

Fig. 2. Localized ^{1}H spectra from primary visual cortex at resting and the three visual stimulation rates (4, 8, and 16 Hz). The lactate peaks are shown at 1.33 ppm.

The second finding supports the ANLS hypothesis construct of two metabolic pathways (oxidative and nonoxidative) that are coexisting, dissociable, and serve different purposes. Oxidative metabolism is predominantly neuronal and supports ATP production for the release of neurotransmitters, whereas nonoxidative metabolism mainly occurs in astrocytes and supports Glu-Gln recycling and induces lactate-mediated hyperemia (see the following paragraph). Even though the percentage increases in lactate concentration were far more than that of CMRO$_2$, the energy demand (i.e., J$_{ATP}$) was predominantly (approximately 98%) met through oxidative metabolism in all stimulation conditions. However, the dramatic increase in lactate concentration indicates that glucose metabolism shifts toward the nonoxidative pathway during neuronal activation. This finding was consistent with the observation of tasked-induced declines in oxygen-glucose index (calculated as CMRO$_2$ / CMR$_{Glc}$) reported in other studies (36). Nonetheless, the energy demand is still largely met through the oxidative pathway (aerobic ATP yield has a 19/3 coefficient compared with anaerobic yield; Eq. **5**). More than 97% of J$_{ATP}$ was supported by oxidative metabolism during all three levels of the visual stimulation (Tables 1 and 2). As a result, changes in CMRO$_2$ and J$_{ATP}$ were linearly coupled (Fig. 4*A*), consistent with previous findings (refs. 22, 37; similar results shown in figure 6 of ref. 22). However, unlike the other physiological variables measured (e.g., BOLD, CBF, CBV, CMRO$_2$ and [Lac]), the effect of stimulus rate on %ΔJ$_{ATP}$ did not achieve statistical significance ($F = 0.2$), despite a similar effect size. This lack of significance is best attributed to additive error terms, as calculation of %ΔJ$_{ATP}$ incorporates several other independent variables, each of which have measurement errors (Eq. **5**).

The third finding agrees with PET reports that %ΔCBF correlates well with %ΔJ$_{Lac}$, but not with %ΔCMRO$_2$ (13, 22, 29). This finding is consistent with the ANLS model prediction that a portion of the lactate produced by astrocytic anaerobic glycolysis is released into the blood. The increased lactate:pyruvate and NADH:NAD^+ ratios in blood then activate the nitric oxide signaling pathway, increasing CBF (7, 38, 39). It should be noted, however, that astrocytic glycolytic metabolism is not the sole mechanism mediating the CBF response. Activation-induced CBF increases are also mediated by Ca^{2+}, K^+, and adenosine signaling pathways (40–42). Future studies will determine the relative contributions of these (and other) signaling pathways mediating the CBF response.

Table 2. Calculated ATP production and its related oxidative versus nonoxidative contributions

Rate	$J_{ATP\ (a)}$, μmol/g/min	ΔJ_{ATP}, μmol/g/min	ΔJ_{ATP}, %	ΔJ_{ATP}, % (aerobic)	ΔJ_{ATP}, % (anaerobic)
4 Hz	13.0 ± 0.2	2.0 ± 0.2	16.7 ± 1.8	97.8 ± 2.0	2.2 ± 2.0
8 Hz	12.6 ± 0.6	1.5 ± 0.6	13.4 ± 5.4	97.6 ± 2.1	2.4 ± 2.1
16 Hz	12.5 ± 0.8	1.4 ± 0.8	12.2 ± 7.2	97.6 ± 2.1	2.4 ± 2.1
F	0.2	0.2	0.2	0.1	0.1
Post hoc	4 = 8 = 16	4 = 8 = 16	4 = 8 = 16	4 = 8 = 16	4 = 8 = 16

Values are means ± SD. The $J_{ATP(r)}$ was determined by **Eq. 2** = 11.1 (μmol/g/min). *F* values were computed by one-way, repeated measures ANOVA. Post hoc testing was performed per condition by Newman-Keuls test, where = indicates $P > 0.5$.

The negative correlation between %ΔCBF and $\%\Delta CMRO_2$ indicates that oxygen demands are not mediating blood flow responses. This agrees with the observation that oxygen consumption remains elevated during the postactivation period after CBF and CBV have returned to baseline (43). Similarly, Mintun et al. (44) used computational modeling to demonstrate that adequate tissue levels of O_2 can be maintained without the need for increased CBF and confirmed with PET that regional increases in CBF during visual stimulation were not affected by hypoxia. Collectively, these observations argue against the hypothesis that task-induced CBF increases are needed to maintain tissue O_2 concentrations or to increase the blood–brain O_2 gradient to stimulate O_2 delivery. Rather, they strongly indicate that task-induced CBF increases are regulated by factors other than local O_2 demand.

The findings presented here are consistent with current models of activation-induced cerebrovascular autoregulation, including the ANLS model. However, theories of neurovascular and neurometabolic coupling are continuously evolving and aspects of the ANLS model remain controversial, such as whether the lactate used by neurons as a substrate arises from astrocytic or neuronal activity (35) and whether lactate is the preferential substrate of neurons for neurotransmission-related energy needs are topics of active debate (reviewed in ref. 45). Further, Brand (28) proposes that oxidative phosphorylation can be elevated without raising oxygen consumption by the means of deactivation of uncoupling protein, which may provide an alternative explanation for relative low levels of $CMRO_2$ change during brain activation. Finally, whether J_{ATP} is constant during continuous stimulation, as assumed in this study, remains as subject of investigation. Further investigations are needed to resolve these issues. In particular, measures of ATP production, quantitative $CMRO_2$, and CMR_{Glc} using other MRI techniques, such as ^{31}P, ^{17}O, and ^{13}C MRS would be important.

In conclusion, we have reported fMRI-derived within-subject, within-session comparisons of %ΔCBF, $\%\Delta CMRO_2$, $\%\Delta J_{Lac}$, and $\%\Delta J_{ATP}$ during graded visual stimulation. Our observations demonstrate that PET and fMRI results can be brought into agreement and, jointly, can inform theories of neurovascular coupling. Our results confirm that the energy demands of acute neuronal activation, although small, are met through oxidative metabolism and that CBF is regulated by factors other than oxygen demand.

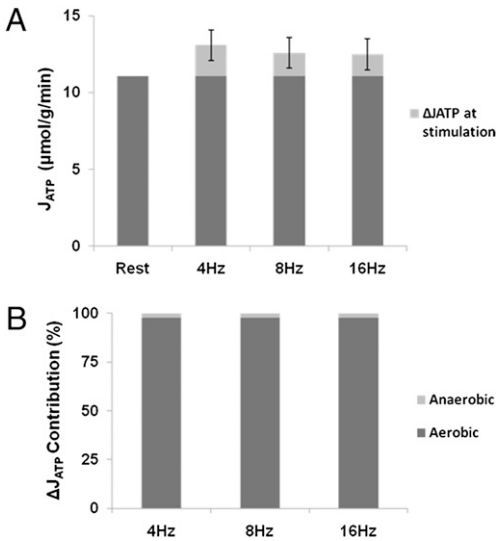

Fig. 3. (*A*) The J_{ATP} at rest and the three levels of visual stimulation. The J_{ATP} rates at activations are independent stimulus rates. The increments at activation are small (1.4–2.0 μmol/g/min) compared with rest (11.1 μmol/g/min). (*B*) The aerobic and anaerobic relative contributions (as percentages) to ΔJ_{ATP}. The ΔJ_{ATP} at the three stimulation rates is predominately a result of aerobic metabolism (approximately 98%, including both neuronal and astrocytic contributions).

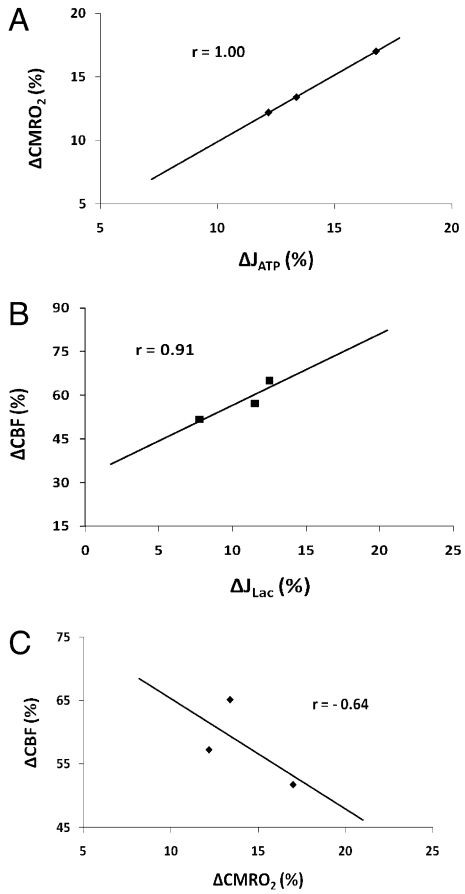

Fig. 4. (*A*) $CMRO_2$–ATP coupling. Significant correlation was shown between $\%\Delta CMRO_2$ and $\%\Delta J_{ATP}$ at the three visual stimulation rates ($r = 1.00$, $P < 0.001$). (*B*) CBF–lactate coupling. Significant correlation was shown between $\%\Delta CBF$ and $\%\Delta J_{Lac}$ at the three visual stimulation rates ($r = 0.91$, $P < 0.001$). (*C*) CBF–$CMRO_2$ coupling. Negative correlation was shown between %ΔCBF and $\%\Delta CMRO_2$ at the three visual stimulation rates ($r = -0.64$, $P = 0.024$).

NEUROSCIENCE

Materials and Methods

Subjects. Twelve healthy volunteers (seven men and five women) between the ages of 22 and 38 y participated in this study. The institional review board of the University of Texas Health Science Center at San Antonio approved the protocol. Written informed consent was obtained from each participant.

fMRI Data Acquisition and Analysis. Experiments were performed on a 3-T Trio MRI scanner (Siemens) with simultaneous, interleaved vascular space occupancy (VASO), arterial spin-labeled (ASL), and BOLD measurements (16, 17). VASO signals were used for determining %ΔCBV (46). A standard transmit/receive head coil was used. A single oblique axial slice (6 mm in thickness) that included the primary visual cortex was chosen for functional imaging. Images were acquired with a field of view of 26 cm and in-plane matrix size of 64 × 64. The echo times (TEs) were 9.4 ms for VASO images, 11.6 ms for ASL images, and 28.1 ms for BOLD images, with a repetition time (TR) of 2,000 ms. The inversion times (TI1; blood nulling point) were 610 ms for VASO images and 1,200 ms for ASL images (TI2). The inversion slab thickness was 100 mm. During an inversion recovery cycle, three images sensitive to VASO, ASL, and BOLD, respectively, were collected. High-resolution T1-weighted anatomical images were obtained with TR/TE/flip angle = 500 ms/11 ms/90°, slice thickness of 6 mm, and in-plane resolution of 1 × 1 mm. During the functional study, subjects were shown a black-and-white radial checkerboard reversing its contrast at frequencies of 4, 8, and 16 Hz. The visual stimulation paradigm consisted of a 4-min visual stimulus at each frequency alternating with 4-min baseline condition (eyes closed). Data were processed and analyzed using MatLab 7 software (MathWorks). For each subject, functional images were coregistered with the anatomical images. Two image pairs acquired after the onset and cessation of each task period were excluded from data analysis to account for the transition time of the hemodynamic response. The VASO image series was obtained by adding the adjacent slab-selective and nonselective images acquired from the first echo in the inversion recovery sequence. The ASL/BOLD image series was obtained by subtracting/adding the adjacent slab-selective and nonselective images from the second/third echo in the sequence. For functional studies, the images (VASO, ASL, and BOLD) acquired during the resting period (4 min) were regarded as baseline images. Student *t* tests were used to compare "baseline" and each frequency "stimulus" signals. The threshold was set to $t = 3.0$ ($P < 0.005$). For each subject, the VASO, ASL, and BOLD functional maps as well as the high-resolution T1-weighted anatomical images were normalized to a standard brain coordinance (Talairach space). The functional maps were then registered to the anatomical images using a convex Hull algorithm (47). Only those common activation areas (in a total volume of 10.1 ± 1.4 cm^3 that includes 120 ± 16 voxels) that passed the statistically significant threshold for all of the VASO, ASL, and BOLD functional maps across all three visual stimulation frequencies were used for calculating the average values of the %ΔCBV, %ΔCBF, and %Δ BOLD, respectively. The three functional quantities were then used to calculate the %ΔCMRO2 (12, 14–17):

$$\%\Delta CMRO_2 = \left(1 - \frac{(\%\Delta BOLD)}{M}\right)^{\frac{1}{\beta}} \cdot (1 + \%\Delta CBV)^{-\frac{1}{\beta}} \cdot (1 + \%\Delta CBF) - 1 \qquad [1]$$

where β is 1.5. M is the basal BOLD relaxation rate (12), determined typically by hypercapnia challenge, as follows. Mild hypercapnia was induced (5% CO_2, 20% O_2, balance N_2) through a nonrebreathing face mask with 1 block of 4 min off/4 min on. End-tidal CO_2 was monitored by means of a nasal cannula with an aspirator. The sequence and imaging parameters were identical to those used in functional studies.

Hydrogen H 1 NMR Data Acquisition and Analysis. Following the fMRI study, the in vivo ^{1}H NMR spectra were obtained using the point-resolved spectroscopy localization approach with a TR and TE of 2,000 ms and 30 ms, respectively. The spectral width was 24 Hz. A voxel of interest was positioned within the primary visual cortex (V1) centered on the calcarine fissure. The voxel of interest was 25 × 21 × 30 mm for a volume of 15.8 cm^3. Visual stimulation was performed as described earlier. The paradigm consisted of 4 min (120 averages) visual stimulus at each frequency alternating with 4 min baseline condition. Data (i.e., free induction decay) for every 120 averages were summed in blocks and further processed using Nuts NMR data processing software (Acorn NMR), including a Fourier transform, frequency correction, phase correction, and baseline correction of the free induction decay. Lactate concentrations during resting and activation states were determined from the ratio of intergraded intensities centered at 1.33 ppm and the *N*-acetylaspartate resonance at 2.02 ppm. Relative lactate concentration [Δ[Lac](%)] was determined by comparing the activation states to the resting state. ΔJLac(%) was determined with Δ[Lac] divided by intergraded time period (4 min).

J_{ATP} and J_{Lac} Determination. The steady-state $J_{ATP\ (r)}$ and $J_{Lac\ (r)}$ (μmol/g/min) can be determined by the stoichiometric relationships as shown in Eqs. **2** and 3, respectively (22).

$$J_{ATP(r)} = 2CMR_{Glc(r)} + 6CMRO_{2(r)} \qquad [2]$$

$$2CMR_{Glc(r)} = J_{Lac(r)} + \frac{1}{3}CMRO_{2(r)} \qquad [3]$$

where r denotes the resting state. $CMR_{Glc(r)}$ and $CMRO_{2(r)}$ in visual cortex—0.42 μmol/g/min and 1.71 μmol/g/min, respectively—were obtained from the literature (5). By substituting Eq. **3** into Eq. **2**, the $J_{ATP(r)}$ can be rearranged as follows:

$$J_{ATP(r)} = J_{Lac(r)} + \frac{19}{3}CMRO_{2(r)} \qquad [4]$$

With continuous 4 min visual stimulation, it was assumed that J_{ATP} during activation also reached a steady state. The J_{ATP} at three levels of stimulation ($J_{ATP(a)}$) can then be calculated as:

$$J_{ATP(a)} = J_{Lac(r)} \times (1 + \%\Delta J_{Lac}) + \frac{19}{3}CMRO_{2(r)} \times (1 + \%\Delta CMRO_2) \qquad [5]$$

where a denotes activation state for each visual stimulus. The $\%\Delta J_{Lac}$ and %Δ $CMRO_2$ were obtained at each visual stimulation condition.

Statistics. All of the measured variables at the three levels of stimulation were compared with by one-way, repeated-measures ANOVA. Post-hoc testing per condition was done by Newman-Keuls test.

ACKNOWLEDGMENTS. We express our appreciation to Drs. Silvia Mangia and Xiao-Hong Zhu at the University of Minnesota for fruitful discussions and valuable comments. This work was supported by National Institutes of Health and University of Texas Health Science Center at San Antonio General Clinical Research Center Grant M01 RR01346.

1. Roy CS, Sherrington CS (1890) On the regulation of the blood-supply of the brain. *J Physiol* 11:85–158, 17.
2. Kety SS, Schmidt CF (1948) The effects of altered arterial tensions of carbon dioxide and oxygen on cerebral blood flow and cerebral oxygen consumption of normal young men. *J Clin Invest* 27:484–492.
3. Frackowiak RS, Lenzi GL, Jones T, Heather JD (1980) Quantitative measurement of regional cerebral blood flow and oxygen metabolism in man using ^{15}O and positron emission tomography: theory, procedure, and normal values. *J Comput Assist Tomogr* 4: 727–736.
4. Mintun MA, Raichle ME, Martin WR, Herscovitch P (1984) Brain oxygen utilization measured with O-15 radiotracers and positron emission tomography. *J Nucl Med* 25: 177–187.
5. Fox PT, Raichle ME, Mintun MA, Dence C (1988) Nonoxidative glucose consumption during focal physiologic neural activity. *Science* 241:462–464.
6. Fox PT, Raichle ME (1986) Focal physiological uncoupling of cerebral blood flow and oxidative metabolism during somatosensory stimulation in human subjects. *Proc Natl Acad Sci USA* 83:1140–1144.
7. Mintun MA, Vlassenko AG, Rundle MM, Raichle ME (2004) Increased lactate/pyruvate ratio augments blood flow in physiologically activated human brain. *Proc Natl Acad Sci USA* 101:659–664.
8. Prichard J, et al. (1991) Lactate rise detected by ^{1}H NMR in human visual cortex during physiologic stimulation. *Proc Natl Acad Sci USA* 88:5829–5831.
9. Frahm J, Krüger G, Merboldt KD, Kleinschmidt A (1996) Dynamic uncoupling and recoupling of perfusion and oxidative metabolism during focal brain activation in man. *Magn Reson Med* 35:143–148.
10. Ogawa S, et al. (1992) Intrinsic signal changes accompanying sensory stimulation: functional brain mapping with magnetic resonance imaging. *Proc Natl Acad Sci USA* 89:5951–5955.

11. Kwong KK, et al. (1992) Dynamic magnetic resonance imaging of human brain activity during primary sensory stimulation. *Proc Natl Acad Sci USA* 89:5675–5679.
12. Davis TL, Kwong KK, Weisskoff RM, Rosen BR (1998) Calibrated functional MRI: mapping the dynamics of oxidative metabolism. *Proc Natl Acad Sci USA* 95:1834–1839.
13. Vafaee MS, Gjedde A (2000) Model of blood-brain transfer of oxygen explains nonlinear flow-metabolism coupling during stimulation of visual cortex. *J Cereb Blood Flow Metab* 20:747–754.
14. Hoge RD, et al. (1999) Linear coupling between cerebral blood flow and oxygen consumption in activated human cortex. *Proc Natl Acad Sci USA* 96:9403–9408.
15. Hoge RD, et al. (1999) Investigation of BOLD signal dependence on cerebral blood flow and oxygen consumption: the deoxyhemoglobin dilution model. *Magn Reson Med* 42:849–863.
16. Lin AL, et al. (2008) Evaluation of MRI models in the measurement of $CMRO_2$ and its relationship with CBF. *Magn Reson Med* 60:380–389.
17. Lin AL, et al. (2009) Time-dependent correlation of cerebral blood flow with oxygen metabolism in activated human visual cortex as measured by fMRI. *Neuroimage* 44: 16–22.
18. Grubb RL, Jr, Raichle ME, Eichling JO, Ter-Pogossian MM (1974) The effects of changes in $PaCO_2$ on cerebral blood volume, blood flow, and vascular mean transit time. *Stroke* 5:630–639.
19. Ito H, Takahashi K, Hatazawa J, Kim SG, Kanno I (2001) Changes in human regional cerebral blood flow and cerebral blood volume during visual stimulation measured by positron emission tomography. *J Cereb Blood Flow Metab* 21:608–612.
20. Kida I, Rothman DL, Hyder F (2007) Dynamics of changes in blood flow, volume, and oxygenation: implications for dynamic functional magnetic resonance imaging calibration. *J Cereb Blood Flow Metab* 27:690–696.
21. Fox PT, Raichle ME (1984) Stimulus rate dependence of regional cerebral blood flow in human striate cortex, demonstrated by positron emission tomography. *J Neurophysiol* 51:1109–1120.
22. Gjedde A (1997) *Cerebrovascular Disease*, eds Bajter H, Caplan L (Lippincott-Raven, Philadelphia), pp 23–40.
23. Hyder F, et al. (2006) Neuronal-glial glucose oxidation and glutamatergic-GABAergic function. *J Cereb Blood Flow Metab* 26:865–877.
24. Lebon V, et al. (2002) Astroglial contribution to brain energy metabolism in humans revealed by ^{13}C nuclear magnetic resonance spectroscopy: elucidation of the dominant pathway for neurotransmitter glutamate repletion and measurement of astrocytic oxidative metabolism. *J Neurosci* 22:1523–1531.
25. Vafaee MS, et al. (1999) Frequency-dependent changes in cerebral metabolic rate of oxygen during activation of human visual cortex. *J Cereb Blood Flow Metab* 19: 272–277.
26. Mintun MA, Vlassenko AG, Shulman GL, Snyder AZ (2002) Time-related increase of oxygen utilization in continuously activated human visual cortex. *Neuroimage* 16: 531–537.
27. Pellerin L, Magistretti PJ (1994) Glutamate uptake into astrocytes stimulates aerobic glycolysis: a mechanism coupling neuronal activity to glucose utilization. *Proc Natl Acad Sci USA* 91:10625–10629.
28. Brand MD (2005) The efficiency and plasticity of mitochondrial energy transduction. *Biochem Soc Trans* 33:897–904.
29. Gjedde A (2007) *Handbook of Neurochemistry and Molecular Neurobiology Brain Energetics. Integration of Molecular and cellular Processes*, eds Lajtha A, Gibson GE (Springer, Heidelberg), pp 343–400.
30. Zhu XH, et al. (2009) Advanced in vivo heteronuclear MRS approaches for studying brain bioenergetics driven by mitochondria. *Methods Mol Biol* 489:317–357.
31. Pette D (1985) Metabolic heterogeneity of muscle fibres. *J Exp Biol* 115:179–189.
32. Hevner RF, Liu S, Wong-Riley MT (1995) A metabolic map of cytochrome oxidase in the rat brain: histochemical, densitometric and biochemical studies. *Neuroscience* 65: 313–342.
33. Van den Berg C (1986) *Energetics and Human Information Processing*, eds Hockey GRJ, Gaillard AWK, Coles MGH (Nijhoff, Boston), pp 131–135.
34. Vlassenko AG, Rundle MM, Mintun MA (2006) Human brain glucose metabolism may evolve during activation: findings from a modified FDG PET paradigm. *Neuroimage* 33:1036–1041.
35. Gjedde A, Marrett S (2001) Glycolysis in neurons, not astrocytes, delays oxidative metabolism of human visual cortex during sustained checkerboard stimulation in vivo. *J Cereb Blood Flow Metab* 21:1384–1392.
36. Shulman RG, Hyder F, Rothman DL (2001) Cerebral energetics and the glycogen shunt: neurochemical basis of functional imaging. *Proc Natl Acad Sci USA* 98:6417–6422.
37. Mangia S, et al. (2007) Sustained neuronal activation raises oxidative metabolism to a new steady-state level: evidence from ^{1}H NMR spectroscopy in the human visual cortex. *J Cereb Blood Flow Metab* 27:1055–1063.
38. Vlassenko AG, Rundle MM, Raichle ME, Mintun MA (2006) Regulation of blood flow in activated human brain by cytosolic NADH/NAD^+ ratio. *Proc Natl Acad Sci USA* 103: 1964–1969.
39. Ido Y, Chang K, Williamson JR (2004) NADH augments blood flow in physiologically activated retina and visual cortex. *Proc Natl Acad Sci USA* 101:653–658.
40. Takano T, et al. (2006) Astrocyte-mediated control of cerebral blood flow. *Nat Neurosci* 9:260–267.
41. Haddy FJ, Vanhoutte PM, Feletou M (2006) Role of potassium in regulating blood flow and blood pressure. *Am J Physiol Regul Integr Comp Physiol* 290:R546–R552.
42. Soricelli A, et al. (1995) Effect of adenosine on cerebral blood flow as evaluated by single-photon emission computed tomography in normal subjects and in patients with occlusive carotid disease. A comparison with acetazolamide. *Stroke* 26: 1572–1576.
43. Lu H, Golay X, Pekar JJ, Van Zijl PC (2004) Sustained poststimulus elevation in cerebral oxygen utilization after vascular recovery. *J Cereb Blood Flow Metab* 24:764–770.
44. Mintun MA, et al. (2001) Blood flow and oxygen delivery to human brain during functional activity: theoretical modeling and experimental data. *Proc Natl Acad Sci USA* 98:6859–6864.
45. Mangia S, et al. (2009) Metabolic and hemodynamic events after changes in neuronal activity: current hypotheses, theoretical predictions and in vivo NMR experimental findings. *J Cereb Blood Flow Metab* 29:441–463.
46. Lu H, Golay X, Pekar JJ, Van Zijl PC (2003) Functional magnetic resonance imaging based on changes in vascular space occupancy. *Magn Reson Med* 50:263–274.
47. Lancaster JL, et al. (1999) Global spatial normalization of human brain using convex hulls. *J Nucl Med* 40:942–955.